Incommensurate Magnetic Fluctuations in $YBa_2Cu_3O_{6.6}$

Pengcheng Dai,[1] H. A. Mook,[1] and F. Doğan[2]
[1]*Oak Ridge National Laboratory, Oak Ridge, Tennessee 37831-6393*
[2]*Department of Materials Science and Engineering, University of Washington, Seattle, Washington 98195*
(Received 27 May 1997)

We use inelastic neutron scattering to demonstrate that the low-frequency magnetic fluctuations in $YBa_2Cu_3O_{6.6}$ ($T_c = 62.7$ K) change from commensurate to incommensurate on cooling with the incommensurability first appearing at temperatures above T_c. For the energies studied, the susceptibility at incommensurate positions increases on cooling below T_c, accompanied by a suppression of the spin fluctuations at the commensurate points. These results suggest that incommensurate spin fluctuations may be a common feature for all cuprate superconductors. [S0031-9007(98)05428-3]

PACS numbers: 74.72.Bk, 61.12.Ex

One of the most important questions in the study of high-temperature (T_c) cuprate superconductors is the nature of the interplay between the antiferromagnetic (AF) spin fluctuations and superconductivity. Indeed, it is widely believed that the spin dynamical properties of the cuprates are responsible for many of their anomalous transport properties and possibly also the superconductivity. For this reason, the wave-vector ($\mathbf{q}$) and energy (ω) dependence of the spin dynamical susceptibility $\chi''(\mathbf{q}, \omega)$, which can be probed directly by neutron scattering, has been intensively investigated over the last several years [1–10]. What is puzzling, however, is the variation of the results from one cuprate to another. For the single layer $La_{2-x}Sr_xCuO_4$ (214) family, spin fluctuations were found at incommensurate positions from the AF lattice point (π, π) [1,2]. For the bilayer $YBa_2Cu_3O_{7-x}$ [$(123)O_{7-x}$], the situation is less clear. While Rossat-Mignod and co-workers detected only spin fluctuations centered at (π, π) [3,7], Tranquada *et al.* [4] found that the $\mathbf{q}$ dependence of the line shape of $\chi''(\mathbf{q}, \omega)$ for $(123)O_{6.6}$ is more complex than a simple commensurately centered Gaussian [4]. However, no firm conclusion about the commensurability and symmetry of $\chi''(\mathbf{q}, \omega)$ were reached in these experiments. Thus, it is not clear whether the incommensurability in spin fluctuations is specific to the 214 family or an essential property of all cuprate superconductors. A resolution of this issue is important because ultimately, a microscopic theory for high-T_c superconductivity must be able to explain the common features of all cuprate superconductors.

In this Letter, we present inelastic neutron scattering data which resolve the commensurability issue in $(123)O_{6.6}$. We show that the low-frequency spin fluctuations in this material change from commensurate to incommensurate on cooling with the incommensurability first appearing at temperatures above T_c. For the energies studied, the susceptibility at incommensurate positions increases on cooling below T_c, accompanied by a suppression of the spin fluctuations at the commensurate points. Our results therefore indicate that the incommensurability may be a common feature for all cuprate superconductors.

The neutron scattering measurements were made at the High-Flux Isotope Reactor at Oak Ridge National Laboratory using the HB-1 and HB-3 triple-axis spectrometers. The characteristics of our single-crystal sample of $(123)O_{6.6}$ ($T_c = 62.7$ K) were described in detail previously [8]. The major difficulty in studying spin fluctuations in the $(123)O_{7-x}$ system is to separate the magnetic signal from (single and multi) phonon and other spurious processes. While spurious events such as accidental Bragg scattering can be identified by checking the desired inelastic scan in the two-axis mode [4], two approaches can be used to separate magnetic from phonon scattering. The first approach is to perform neutron polarization analysis [11] which, in principle, allows an unambiguous separation of magnetic and nuclear scattering. This method has been successfully employed to identify the magnetic origin of resonance peaks for ideally [5] and underdoped [8,9] $(123)O_{7-x}$. However, this advantage comes at a considerable cost in intensity which makes the technique impractical for observing small magnetic signals. The second approach is to utilize the differences in the temperature and $\mathbf{q}$ dependence of the phonon and magnetic scattering cross sections. While phonon scattering gains intensity on warming due to the thermal population factor, the magnetic signal usually becomes weaker because it spreads throughout the energy and momentum space at high temperatures. Thus, in an unpolarized neutron measurement the net intensity gain above the multiphonon background on cooling at appropriate wave vectors is likely to be magnetic in origin.

Figure 1(a) depicts the reciprocal space probed in the experiment with $\mathbf{a^*}$ ($= 2\pi/a$), $\mathbf{b^*}$ ($= 2\pi/b$) directions shown in the square lattice notation. The momentum transfers (q_x, q_y, q_z) in units of Å^{-1} are at positions $(H, K, L) = (q_x a/2\pi, q_y b/2\pi, q_z c/2\pi)$ reciprocal lattice units (rlu). We first describe measurements made in the (H, H, L) zone. Our search for the magnetic fluctuations was done with the filter integration technique [12]. This technique is effective for isolating scattering from lower dimensional objects and relies on integrating the energy along the wave-vector direction $[0, 0, L]$ perpendicular to the

 0031-9007/98/80(8)/1738(4)$15.00

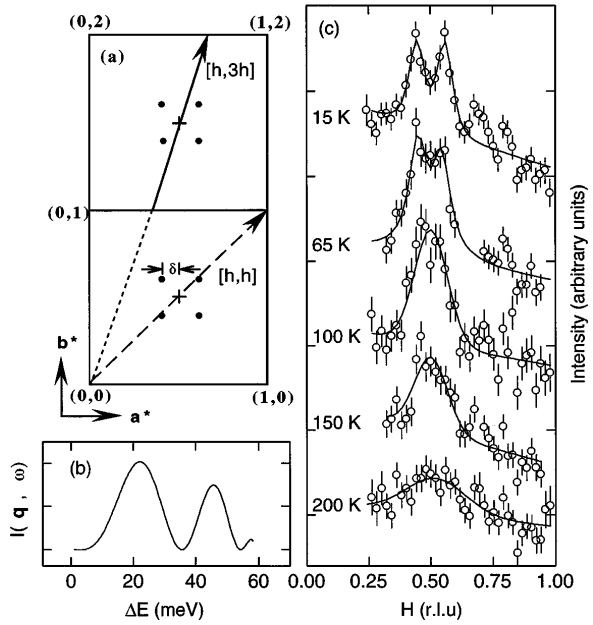

FIG. 1. (a) Diagram of reciprocal space probed in the experiment. The dashed arrow indicates the scan direction with the integrated technique while the solid arrow represents the triple-axis measurements. (b) Calculated scattered intensity $I(\mathbf{q}, \omega)$ as a function of energy transfer. (c) Integrated measurements in which the data at 295 K are subtracted from 200, 150, 100, 65, and 15 K. The data are normalized to the same monitor count. The solid lines in the 100, 150, and 200 K data are fits to single Gaussians and linear backgrounds. The solid lines in the 15 and 65 K data are two Lorentzian-squared peaks on linear backgrounds which best fit the data.

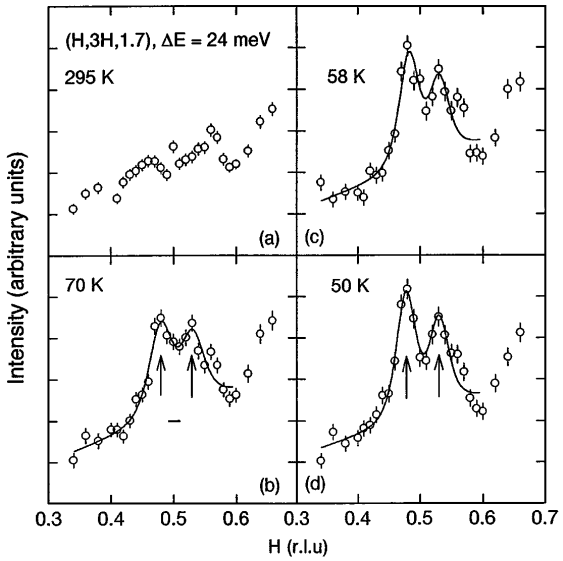

FIG. 2. Triple-axis scans along $(H, 3H, 1.7)$ at 24 meV for (a) 295 K, (b) 70 K, (c) 58 K, and (d) 50 K. Data at 295 K were collected with HB-1 while other scans were taken using HB-3. The weak structures in (a) are most likely due to phonon and/or spurious processes. The horizontal bar shows the resolution along the scan direction and the vertical resolution is 0.14 Å^{-1}. The positions of incommensurability at $H \approx 0.48$ and 0.53 rlu are indicated by the arrows. Solid lines in (b)–(d) are two Lorentzian-squared peaks on a linear background. The increased scattering at $H > 0.6$ rlu is due to phonons.

scan direction $[H, H, 0]$. To estimate the energy integration range of the technique, we note that the scattered intensity for acoustic modulations in $(123)O_{7-x}$ is proportional to the in-plane susceptibility $\chi''(q_x, q_y, \omega)$ [4,13]

$$I(\mathbf{q}, \omega) \propto \frac{k_f}{k_i} |f_{\mathrm{Cu}}(\mathbf{q})|^2 \sin^2\left(\frac{1}{2}\Delta z q_z\right) \times [n(\omega) + 1]\chi''(q_x, q_y, \omega),$$

where k_i and k_f are the initial and final neutron wave numbers, $f_{\mathrm{Cu}}(\mathbf{q})$ is the Cu^{2+} magnetic form factor, Δz (= 3.342 Å) the separation of the CuO_2 bilayers, $\mathbf{q}$ the total momentum transfer ($|\mathbf{q}|^2 = q_x^2 + q_y^2 + q_z^2$), and $[n(\omega) + 1]$ the Bose population factor. The solid line in Fig. 1(b) shows the calculated $I(\mathbf{q}, \omega)$ at (π, π) as a function of energy transfer (along q_z) assuming $\chi''(q_x, q_y, \omega) = F(q_x, q_y)\chi''(\omega) \propto \omega F(q_x, q_y)$ [14]. Although there are two broad peaks in the figure, the observed intensity will mostly stem from fluctuations around the lower energy one ($10 < \Delta E < 30$ meV) because of the decreased resolution volume at large energy transfers. Since room temperature triple-axis measurements show no detectable magnetic peaks at (π, π) below ~40 meV (see Figs. 2 and 3), we have used the integrated scan at 295 K as the background and assumed that the subsequent net intensity gains above the multiphonon background at lower temperatures are magnetic in origin. Figure 1(c) shows the result at different temperatures. At 200 K, the magnetic fluctuations are broadly peaked at (π, π). On cooling to 150 and 100 K, the peak narrows in

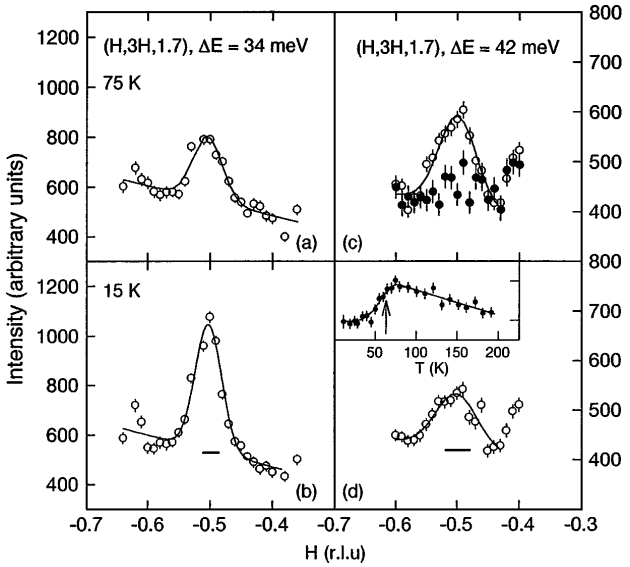

FIG. 3. Constant-energy scans along $(H, 3H, 1.7)$ with energy transfer of 34 meV at (a) 75 K, and (b) 15 K. Identical scans at 42 meV at (c) 295 K (•), 75 K (∘), and (d) 15 K (∘). Inset (•) shows the temperature dependence of the scattering at $(0.5, 1.5, -1.7)$ for $\Delta E = 42$ meV where the arrow indicates T_c. The multiphonon background in the 295 K data has been scaled to the value at 75 K for clarity. The horizontal bars represent instrumental resolution. Solid lines are Gaussian fits to the data.

width and grows in intensity but is still well described by a single Gaussian centered at (π, π). At 65 K, the data show a flattish top similar to previous observations [4]. Although detailed analysis suggests that the profile is better described by a pair of peaks (Lorentzian or Lorentzian-squared line shape) than a single Gaussian, the most drastic change in the profile comes in the low-temperature superconducting state. Rather than previously observed single peak, two peaks at positions displaced by $\pm\delta$ (0.057 $\pm$ 0.006 rlu) from $H = 0.5$ are observed, accompanied by a drop in the spin fluctuations at the commensurate position. The observation of sharp incommensurate peaks with the filter integration technique suggests that the incommensurability must be weakly energy dependent in the integration range.

Although the integration technique is excellent for finding weak peaks from the scattering of lower dimensional objects, it is important to confirm the result with triple-axis measurements and to determine the symmetry of the incommensurability. For this purpose, we have realigned the sample in the $(H, 3H, L)$ zone. If the 15 K profile in Fig. 1(c) stems from an incommensurate structure with peaks at $(0.5 \pm \delta, 0.5 \pm \delta)$ [see Fig. 1(a)], scans along the $[H, 3H]$ direction are expected to peak at $H = 0.477$ and 0.523 rlu for $\delta = 0.057$. On the other hand, if the underlying symmetry is identical to that of 214 [rotated 45° from Fig. 1(a)], the incommensurability in a $[H, 3H]$ scan should occur at $H = 0.466$ and 0.534 rlu. Figure 2 summarizes the result at 24 meV [15]. The scattering at room temperature shows no well-defined peak around (π, π), but at 70 K a two peak structure emerges. On cooling below T_c, the spectrum rearranges itself with a suppression of fluctuations at a commensurate point accompanied by an increase in intensity at incommensurate positions. The wave vectors of the peaks in the $[H, 3H]$ scan are consistent with either the incommensurate peaks shown in Fig. 1(a) or those found for the 214 materials. However, we stress that other structures may also explain the data and more precise measurements are necessary before a conclusive identification of the underlying structure can be made.

In previous work, superconductivity was found to induce a strong enhancement in $\chi''(\mathbf{q}, \omega)$ at (π, π) for ideally [3,5,6] and underdoped [8–10] $(123)O_{7-x}$ at the resonance positions. Although the intensity gain of the resonance below T_c is accompanied by a suppression of fluctuations at frequencies above it for the underdoped compounds [8,9], no constant-energy scan data are available at energies above the resonance. In light of the present result at 24 meV for the $(123)O_{6.6}$ sample which has a resonance at 34 meV [8], it is important to collect data at these frequencies. Thus, we undertook additional measurements with improved resolution (collimation of 50′-40′-40′-120′) in the hope of resolving possible incommensurability at high energies. Figures 3(a) and 3(b) suggest that the fluctuations at the resonance energy are commensurate above and below T_c with no appreciable change in width. For an energy above the resonance (42 meV), the scan is featureless at room temperature but shows a well-defined peak centered at (π, π) at 75 K. Although superconductivity suppresses the magnetic fluctuations [see inset of Fig. 3(d)], the **q** dependence of the line shape cannot be conclusively determined due to the poor instrumental resolution at this energy. Unfortunately, further reduction in resolution volume is impractical due to the concomitant drop in the scattering intensities.

Since the earlier polarized neutron work [8] has shown that for $(123)O_{6.6}$ the 34 meV resonance is the dominant feature of $\chi''(\mathbf{q}, \omega)$ at (π, π) in the low-temperature superconducting state, it is important to compare the newly observed incommensurate peaks to the intensity gain of the resonance. Figure 4 shows the difference spectra between 15 and 75 K at frequencies below and above the resonance. In the energy and temperature range of interest (15 to 75 K), the phonon scattering changes negligibly and the Bose population factor $[n(\omega) + 1]$ modifies the scattered intensity at high temperatures by only 3% at 24 meV and less at higher energies. Therefore, the difference spectra in the figure can be simply regarded as changes in the dynamical susceptibility, i.e., $\chi''(15\ \text{K}) - \chi''(75\ \text{K})$.

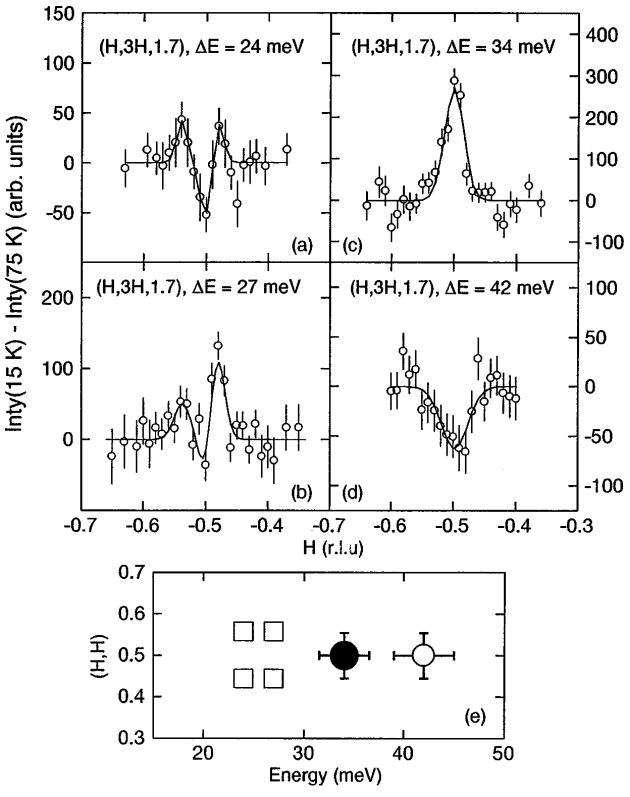

FIG. 4. Difference spectra along $(H, 3H, 1.7)$ between low temperature ($<T_c$) and high temperature ($\approx T_c$ + 12 K) at (a) 24 meV, (b) 27 meV, (c) 34 meV, and (d) 42 meV. All data were taken with the same monitor units. Solid lines are guides to the eye. (e) Summary of triple-axis measurements. Open squares indicate incommensurate positions. Solid and open circles are the resonance and fluctuations at 42 meV, respectively. The error bars show the energy resolution and the intrinsic **q** width (FWHM).

Inspection of Figs. 4(a) and 4(b) reveals that the susceptibility at the incommensurate positions increases on cooling from the normal to the superconducting state, accompanied by a suppression of fluctuations at the commensurate point. Comparison of Fig. 4(c) to Figs. 4(a) and 4(b) indicates that the net gain in intensity at the incommensurate positions below T_c is much less than that of the resonance. For an energy transfer of 42 meV, the intensity drop appears uniform throughout the measured profile; however, instrumental resolution may mask any possible incommensurate features. Figure 4(e) plots a summary of the triple-axis measurements in superconducting state. Although there are only two constant-energy scans for frequencies below the resonance, these data nevertheless confirm the result of the integrated technique.

To place our work in proper context, it is useful to compare the results with various theoretical predictions. If the $(123)O_{7-x}$ system is indeed a d-wave superconductor, d-wave gap nodes could yield incommensurate peaks [16] and the scattering of $(123)O_{6.6}$ is expected to change from commensurate in the normal state to incommensurate in the superconducting state [17]. In this scenario, the susceptibility at incommensurate positions should increase on cooling below T_c for all frequencies below the d-wave gap [17,18]. Our preliminary triple-axis measurements [19] show that spin fluctuations at 16 meV are also incommensurate in the normal state, but on cooling below T_c these fluctuations are suppressed. At present, it remains unclear how to reconcile *this* simple d-wave picture with these results, or perhaps even more problematical, with the appearance of the incommensurate fluctuations at temperatures above T_c.

Alternatively, the observed incommensurate peaks may be viewed as the signature of a stripe phase. Tranquada *et al.* [20] have argued that the incommensurability in 214 may be associated with the spatial segregation of charge or charge density wave correlations [21]. However, if the idea of dynamical microphase separation in the CuO_2 plane asserted by Emery and Kivelson [22] is relevant for the high-T_c superconductivity, one would expect incommensurate spin fluctuations in other cuprate superconductors. The observation of such fluctuations in $(123)O_{7-x}$ is consistent with this picture. Unfortunately, there are no explicit predictions about the incommensurate structure in $(123)O_{7-x}$ from a stripe model that can be directly compared with our experiments.

Finally, previous interpretations of NMR experiments have assumed that AF spin fluctuations in $(123)O_{7-x}$ are commensurate and the spin correlation length ξ is temperature independent [23]. Our data suggest a reconsideration of these assumptions, particularly in view of the apparent contradiction between the results of NMR and neutron scattering experiments [24].

We thank G. Aeppli, V. J. Emery, S. M. Hayden, K. Levin, and D. Pines for helpful discussions. We have also benefited from fruitful interactions with J. A. Fernandez-Baca, R. M. Moon, S. E. Nagler, and D. A. Tennant. This research was supported by the U.S. DOE under Contract No. DE-AC05-96OR22464 with Lockheed Martin Energy Research Corp.

[1] S-W. Cheong *et al.,* Phys. Rev. Lett. **67**, 1791 (1991); T. E. Mason *et al., ibid.* **77**, 1604 (1996).
[2] K. Yamada *et al.,* Phys. Rev. Lett. **75**, 1526 (1995).
[3] J. Rossat-Mignod *et al.,* Physica (Amsterdam) **185C**, 86 (1991).
[4] J. M. Tranquada *et al.,* Phys. Rev. B **46**, 5561 (1992); B. J. Sternlieb *et al., ibid.* **50**, 12 915 (1994).
[5] H. A. Mook *et al.,* Phys. Rev. Lett. **70**, 3490 (1993).
[6] H. F. Fong *et al.,* Phys. Rev. Lett. **75**, 316 (1995).
[7] L. P. Regnault *et al.,* Physica (Amsterdam) **213B**, 48 (1995).
[8] P. Dai *et al.,* Phys. Rev. Lett. **77**, 5425 (1996).
[9] H. F. Fong *et al.,* Phys. Rev. Lett. **78**, 713 (1997).
[10] P. Bourges *et al.,* Europhys. Lett. **313**, 38 (1997).
[11] R. M. Moon *et al.,* Phys. Rev. **181**, 920 (1969).
[12] H. A. Mook *et al.,* Phys. Rev. Lett. **77**, 370 (1996).
[13] The time-of-flight measurements at the ISIS pulsed spallation source [see, for example, S. M. Hayden *et al.,* Phys. Rev. B **54**, R6905 (1996); and cond-mat/9710181] on the sample show that the optical modes appear first at 60 ± 5 meV, thus it is sufficient to model the magnetic fluctuations with the acoustic modulation for the energy range probed in the present experiment.
[14] Here we have adopted the notation of Ref. [4]. The expression $\chi''(\omega) \propto \omega$ is valid for $\omega \rightarrow 0$ (see, for example, Ref. [24]) and we have extended it to give an estimate of the integration range.
[15] In Ref. [8], we have observed a drop in magnetic signal at (π, π). Unfortunately, the polarized constant-energy scan at 24 meV [see Fig. 2(b) of Ref. [8]] did not pick up the incommensurate feature described in this work due to limited intensity of the technique.
[16] J. P. Lu, Phys. Rev. Lett. **68**, 125 (1992).
[17] Y. Zha *et al.,* Phys. Rev. B **47**, 9124 (1993).
[18] N. Bulut and D. J. Scalapino, Phys. Rev. B **47**, 3419 (1993).
[19] P. Dai, H. A. Mook, and F. Doğan, Physica B (to be published).
[20] J. M. Tranquada *et al.,* Nature (London) **375**, 561 (1995); Phys. Rev. B **54**, 7489 (1996); Phys. Rev. Lett. **78**, 338 (1997).
[21] J. Zaanen and O. Gunnarsson, Phys. Rev. B **40**, 7391 (1989); U. Löw *et al.,* Phys. Rev. Lett. **72**, 1918 (1994); C. Castellani *et al., ibid.* **75**, 4650 (1995).
[22] V. J. Emery and S. A. Kivelson, Physica (Amsterdam) **209C**, 597 (1993); **235**, 189 (1994).
[23] See, for example, J. Bobroff *et al.,* Phys. Rev. Lett. **79**, 2117 (1997).
[24] Y. Zha *et al.,* Phys. Rev. B **54**, 7561 (1996); C. Berthier *et al.,* J. Phys. I (France) **6**, 2205 (1996).